Title:
Revisiting face-to-hand area remapping in the human primary somatosensory cortex after a cervical spinal cord injury

Authors:
Paige Howell[1,2,3], Finn Rabe[1,3], Charlotte Meneghin[1], Simon Schading-Sassenhausen[2,3], Harshal Arun Sonar[4], Jamie Paik[4], Patrick Freund[2,3], Nicole Wenderoth[1,3], Sanne Kikkert[1,2,3]

Affiliations:
[1] *Neural Control of Movement lab, Department of Health Sciences and Technology, ETH Zürich, Zürich, Switzerland*
[2] *Spinal Cord Injury Center Balgrist, University Hospital Zürich, University of Zürich, Zürich, Switzerland.*
[3] *Neuroscience Center Zurich, University of Zurich and ETH Zurich, Zürich, Switzerland.*
[4] *Reconfigurable Robotics Lab, École polytechnique fédérale de Lausanne, Lausanne, Switzerland.*

Abstract:

Spinal cord injury (SCI) leads to profound disruptions in sensorimotor processing. Seminal research in non-human primates suggests that this deprivation of sensory input causes functional remapping within the primary somatosensory cortex (S1). Crucially, cortical somatotopic representations of deprived body parts, such as the hand in cervical SCI, become responsive to touch on intact body parts, such as the face. However, in humans, the evidence for cortical remapping following SCI remains inconclusive.

Here, sixteen chronic cervical SCI patients (mean age ± s.e.m. = 52.4 ± 3.5 years; 1 female) and 21 able-bodied controls (age: 49.9 ± 3.4; 2 females) participated in two experiments in which we used a systematic and sensitive approach to determine the full extent of face-to-hand area remapping. In Experiment 1, we employed a lip movement fMRI paradigm, as previously used in human remapping studies. In Experiment 2, we investigated the full architecture of S1 face reorganisation through vibrotactile stimulation of the forehead, lips and chin. Firstly, we assessed whether the level of face activity in the anatomical S1 hand area was increased in SCI patients compared to controls. Secondly, we evaluated potential cortical shifts in peak face activity using geodesic distances. Thirdly, we used representational similarity analysis, where, in the instance of S1 face-to-hand remapping, we anticipated larger representational distances (i.e., more somatotopic information) between the different face sites in the S1 hand area. Finally, we explored what clinical characteristics may be driving face-to-hand area remapping.

Our results revealed no significant differences between control participants and tetraplegic patients in any of our three markers for reorganisation during lip movement (Experiment 1) or vibrotactile stimulation (Experiment 2). Furthermore, we found no significant correlations between remapping and the clinical traits of the SCI patients.

These findings suggest that cortical reorganisation is not apparent in human cervical SCI patients. As such, the extent of face-to-hand area reorganisation after a human SCI appears to differ fundamentally from what has been observed in experimental models of SCI. Beyond providing essential insights into the limitations of cortical reorganisation in humans, these findings call for a reassessment of rehabilitation strategies based on the assumption of face-to-hand reorganisation after an SCI.

1. Introduction

A spinal cord injury (SCI) profoundly alters the sensorimotor system, disrupting both muscle function and sensation in the limbs and torso below the level of injury[1]. Seminal non-human primate studies demonstrate that this loss of sensation leads to extensive remapping in brain areas containing detailed map-like body representations, such as the primary somatosensory cortex (S1)[2-4]. Consequently, cortical areas that are deprived of sensory inputs, such as those from the hand, become responsive to touch on intact body parts, such as the face[5]. While animal models of SCI have consistently demonstrated remapping in S1[4,6-9], whether similar remapping occurs after human SCI remains inconclusive (see Melo et al. [10] for a review).

Several studies have demonstrated evidence in favour of S1 remapping after human SCI, where activation from touch or movement of intact body parts is observed in or shifted towards the deprived S1 area[11-15]; though see[16-18]. However, most of these studies were done in thoracic or lumbar SCI patients[14-16,18]. While the majority of animal, and specifically non-human primate, work has focused on S1 face-to-hand remapping after cervical SCI, evidence of similar remapping in humans is highly mixed. Despite a lack of compelling evidence in favour of face-to-hand remapping, the assumption of drastic reorganisation in humans remains highly influential in the neuroscientific literature and the clinic[3,19]. Reorganisation of affected cortical areas is thought to drive both recovery of function and the formation of maladaptive neuronal circuitry that relates to neuropathic pain[20-23]. Given this proposed role of S1 reorganisation in determining clinical outcomes, it is essential to determine whether the human S1 cortex does, in fact, reorganise after an SCI.

Several factors may explain the inconsistency of face-to-hand area remapping results in humans compared to non-human primates. Firstly, studies in non-human primates have primarily reported chin-to-hand area reorganisation in S1[4,6,7,24], whereas human studies have focused on mouth-to-hand area reorganisation[12,16,18]. If cortical reorganisation is limited to regions neighbouring the deprived hand area, then differences in facial somatotopy between non-human primates and humans may account for the lack of mouth-to-hand area reorganisation. Indeed, the S1 face representation is inverted in non-human primates, with the chin neighbouring the hand representation[25]. In contrast, human studies show that the forehead is positioned closest to the hand representation[26-28]. Secondly, there is no methodological consensus in the literature on how best to quantify reorganisation in humans. While tactile stimulation protocols have been employed in non-human primates, human studies often use movement paradigms due to the difficulty of providing tactile face stimulation in an MRI environment[12,29-32]. Moreover, most studies quantify reorganisation using Euclidean distance measures[16-18,32], which do not account for the folded anatomy of the cortical surface. Alternatively, geodesic distances would provide a more anatomically and functionally accurate measure of the spatial relationship between hand and face cortical representations[33]. Lastly, researchers studying human reorganisation have classically relied on univariate analysis techniques. However, multivariate methods may be more effective than univariate approaches for studying cortical remapping, as they evaluate the entire multidimensional activity pattern elicited by stimuli, enabling the detection of subtle representational changes that may not manifest as differences in overall activity levels. To date, only Root et al. [27] have utilised a multivariate representational similarity analysis (RSA) approach to study reorganisation in this context. These methodological discrepancies highlight the need for more systematic and sensitive approaches to assess reorganisation in humans.

Therefore, in this study, we conducted an in-depth investigation to reassess the assumption of face-to-hand area remapping in the human S1 cortex following SCI using fMRI and extensive uni- and multivariate analysis techniques. In Experiment 1, we replicated previous studies using a lip movement paradigm to characterise mouth-to-hand area reorganisation. In Experiment 2, we more closely mimicked non-human primate work by using vibrotactile stimulation of the forehead, lips, and chin to characterise S1 face-to-hand reorganisation in detail. By stimulating multiple face parts, we ensured that the cortical neighbour of the hand area was not overlooked. Moreover, for a comprehensive analysis, we assessed reorganisation using both univariate and multivariate analysis approaches. We hypothesised that if face representations reorganise into the S1 hand area in human cervical SCI patients, we would find increased face activity in the S1 hand area. Alternatively, if face representations shift toward but do not fully invade the deprived S1 hand area, we would detect a shift in the activity elicited by lip movements and/or face stimulation in SCI patients relative to controls. Furthermore, we expected to find more distinct face information in the S1 hand area, reflected by higher representational dissimilarity scores in SCI patients compared to controls. Given the greater sensitivity of multivariate approaches to detect subtle changes, we further explored correlations with these results to better understand what clinical and behavioural determinants may drive reorganisation in the human somatosensory cortex. By combining several measures of reorganisation, we aimed to provide a systematic and robust framework to assess face-to-hand reorganisation in human cervical SCI patients.

2. Materials and methods

2.1 Participants

Seventeen chronic (i.e., >6 months post-injury) cervical SCI patients and twenty-one age- sex- and handedness-matched able-bodied control participants (mean age ± s.e.m. = 49.9 ± 3.4; 2 females; 3 left-handers) participated in this study. Patient inclusion criteria were as follows: Aged 18-75 years, no MRI contraindications, at least 6 months post cervical SCI, no neurological impairment or body function impairments not induced by SCI, and able to provide informed consent. One patient was excluded after data collection upon confirming their injury was thoracic, not cervical, resulting in a final sample of sixteen cervical spinal cord injury patients (mean age ± s.e.m. = 52.4 ± 3.5 years; 1 female 3 left-handers; years since injury ranging from 6 months to 37 years; see Table 1).

Control participant inclusion criteria were as follows: Aged 18-75 years, no MRI contraindications, no impairment of body function induced by SCI, no neurological illness, no hand impairments, and able to provide informed consent. Data of one control participant was excluded from the analysis of experiment 1 due to corruption of their fMRI data during data acquisition. Ethical approval was granted by the Kantonale Ethikkommission Zürich (EK-2018-00937), and written informed consent was obtained prior to the study onset. This study is registered on clinicaltrials.gov under the number NCT03772548. A portion of the control participant dataset used in Experiment 2 has been previously published (see [26] for details).

Sex (m/f)	Age (range)	Time since injury (range)	AIS grade (A/B/C/D)	Neurological level of injury (range)	Total GRASSP score (range)
15/1	31-70	0.5-37	5/0/2/9	(C1-C7)	22-188

Table 1: Aggregated patient demographic and clinical details. Sex: M = male, F = female; Age = age in years; Time since injury = Time since injury in years; AIS grade = American Spinal Injury Association (ASIA) impairment Scale grade defined based on the International Standards for Neurological Classification of Spinal Cord Injury (ISNCSCI): A = complete, B = sensory incomplete, C = motor incomplete, D = motor incomplete;

Neurological level of injury = defined based on the ISNCSCI; GRASSP score = Graded Redefined Assessment of Strength, Sensibility and Prehension (able-bodied score: 232 points).

2.2 Clinical characterisation

Behavioural testing was conducted in a separate session. We classified each patient's injury completeness and impairment level using the International Standards for Neurological Classification of Spinal Cord Injury (ISNCSCI). In addition, we used the Graded Redefined Assessment of Strength, Sensibility and Prehension (GRASSP) assessment to define the sensory and motor integrity of the upper limbs[34]. We determined each patient's most impaired upper limb according to the maximum GRASSP score for each limb. Finally, to assess pain, we asked participants to report their average pain levels over the past week.

2.3 Experimental design

Experiment 1

In experiment 1, we investigated face-to-hand area remapping in S1 using a lip movement paradigm. We designed a blocked fMRI experiment with three self-paced movement conditions: (1) face movement (continuous jaw clenching and self-paced lip pursing), (2) left-hand open-and-closing, and (3) right-hand open-and-closing. Note that the hand movement conditions were not included in the analysis of the current manuscript (see [35] for details).

We instructed participants to focus on a green fixation cross on a black screen throughout the scan. Participants viewed the screen via a mirror mounted on the head coil with the instructions 'left hand', 'right hand', 'face', and 'rest' displayed in white text behind the green fixation cross. Each movement block lasted 12 seconds, followed by a 6-second rest block. Each condition was repeated 8 times per run in a counterbalanced order. In total, we acquired four runs, each with a different block order, resulting in a total duration of 28 minutes and 48 seconds. Instructions were delivered using Psychtoolbox (v3) implemented in Matlab (v2014b). Head motion was minimised using over-ear MRI-safe headphones or padded cushions.

Experiment 2

In experiment 2, we investigated face-to-hand area remapping using a vibrotactile face stimulation paradigm. We used a newly developed MRI-compatible tactile stimulation device that employs soft pneumatic actuator (SPA) technology to provide focal, suprathreshold vibrotactile stimulation to specific parts of the face. We previously described our device setup and stimulation paradigm in Kikkert et al. [26]. However, for accessibility, we reiterate the stimulation setup below.

We used a soft, skin-like interface that uses modulated pneumatic pressure to provide vibrotactile stimulation. The soft pneumatic actuators (SPA) skins are made of MR-safe silicone (Dragon Skin 30®, Smooth On Inc., USA), and the amplitude is controlled by varying the internal pressure as well as its actuation frequencies[36,37]. The SPA system consists of the following components: a stimulus computer, a portable air compressor, a portable pneumatic setup, and pneumatic tubes. We controlled stimulation intensity and frequency using a stimulus computer in the scanner control room. An air compressor, also placed in the scanner control room, provided airflow to a pressure regulator that was controlled by a microcontroller in the portable pneumatic setup. The stimulation intensity could be adjusted using the pressure regulator and an array of high-speed pneumatic valves that were driven by high-power switches and inputs from the microcontroller. A 50 mm diameter hole in the RF shielding wall then carried the 5–6 m long and 4 mm thick tubes (2.8 mm I.D.) to the SPA-skin in the fMRI scanner

room. The entire SPA setup is optimised for meeting the fMRI specifications for the selection of individual components, as discussed in detail by Joshi et al. [38].

We attached ring-shaped SPA-skins to the forehead (~1cm above the eyebrow), above the upper lip, and on the chin (Figure 2A). We selected these sites to ensure that an SPA-skin was placed on each of the face areas innervated by the three trigeminal nerve branches. We took special care not to place SPA-skins on the areas that lie at the border of trigeminal nerve innervations. To ensure good grounding of the SPAs on the face, we placed in-house 3D printed plates on top of the SPA-skins and used a custom-made fabric face mask to apply light pressure to the SPA-skins. A further SPA-skin was attached to the ipsilateral thumb using adhesive tape. It is important to note that we did not include the thumb condition in the analysis of this manuscript, as the resulting activity in SCI patients differs largely from controls due to the impaired sensation and diminished (or absent) sensory thumb inputs travelling past the spinal injury.

Participants viewed a visual display positioned at the head of the scanner bore through a mirror mounted on the head coil. To cue the participant which location would be stimulated, a white text cue ("forehead", "lips", "chin", and "thumb") appeared on a black screen 0.8s prior to stimulation onset and remained on the screen until stimulation offset. Participants were instructed to attend to the highlighted stimulation location while the cue was displayed. Stimulation was presented for 8s at 8Hz, consisting of 400ms bursts of stimulation 'on' periods followed by a 100ms 'off' period to minimise peripheral adaptation. To ensure stable attention during the fMRI runs, stimulations were interrupted in a small percentage of the stimulation blocks (10-20% of blocks per run). In these interrupted stimulation trials, stimulation was provided for 4s, after which a 2s silent period was introduced, followed by another 2s of stimulation. We ensured that the interrupted stimulation trials were equally distributed across the stimulation locations within each run. Participants were instructed to count the number of interrupted stimulation trials and verbally report this at the end of each run.

To ensure that the BOLD response induced by stimulation was not confounded by differences in stimulation intensity across the stimulation locations, we aimed to match sensation intensity across stimulation locations prior to the fMRI runs. We performed a stimulation intensity matching task in which participants first determined the optimal stimulation intensity for the forehead. The forehead was selected as the reference location because it is innervated by the fewest mechanoreceptors and was, therefore, assumed to be the least sensitive stimulation location[39]. Participants were instructed to identify an optimal stimulation intensity that was as strong as possible while remaining focal (i.e., localised without spread to adjacent skin), comfortable, and stable throughout the 8s stimulation period (i.e., with minimal peripheral adaptation). Participants used a button box to indicate whether the intensity should be increased, decreased, or left unchanged. Based on these responses, the air pressure provided to the SPAs was adjusted in steps of 5 kPa to increase or decrease stimulation intensity or remain stable. If a participant indicated twice in succession that the stimulation intensity should not change, the pressure for the forehead was set for all subsequent fMRI tasks. The current SPA-skins design allows for a pressure input range of 20-80 kPa while producing 0.1-1 N force feedback, suitable for the human tactile perception range[40,41]. Once the optimal stimulation intensity was set for the reference location, participants were asked to match the stimulation intensity for the other stimulation locations to that of the forehead. To facilitate this matching, participants were initially given 8s of stimulation on the forehead, immediately followed by stimulation of one of the other locations. Participants were instructed to adjust the intensity of the second location to match the intensity of the reference location as closely as possible. As

before, if the participant indicated twice that the stimulation intensity should remain unchanged, the pressure for that stimulation location was set at this level for all fMRI tasks.

To uncover face somatotopy, we used a blocked design consisting of five conditions: stimulation of the forehead, lips, chin, and thumb, as well as a rest condition (no stimulation). Within each participant, we consistently tested either the right side of the face and right thumb or the left side of the face and left thumb. The side tested was always ipsilateral to the most impaired side of the body for each SCI patient. We then matched the tested sides in controls to those in patients. The visual cue during the face stimulation blocks was as described above and the presentation of the word "Rest" indicated the rest condition. Each condition had a block duration of 8.8s and was repeated eight times per run in a counterbalanced order. Each run comprised a different block order and had a duration of 6min and 7.4s. We acquired four blocked design runs, with a total duration of 24min and 29.6s. Instructions and stimulations were delivered using Psychtoolbox (v3) implemented in Matlab (v2014b). Matlab communicated with the Arduino board implemented in the SPA controller set-up via a serial port over a proprietary protocol. Head motion was minimised using over-ear MRI-safe headphones or padded cushions.

2.4 MRI acquisition

We acquired MRI data with a 3 Tesla Philips Ingenia system (Best, The Netherlands) and a 15-channel HeadSpine coil. However, in the instance that the 15-channel coil was unsuitable due to head size limitations, a 32-channel HeadSpine coil was used instead. We acquired an anatomical T1-weighted structural scan with the following acquisition parameters: TE: 4.4ms; TR: 9.3ms; flip angle: 8˚; resolution: 0.75mm^3. For task-fMRI, we used an echo-planar-imaging (EPI) sequence with partial brain coverage.

For experiment 1, we centred 32 sagittal aligned parallel to the floor of the fourth ventricle, with coverage over S1, the thalamus, and the brainstem. The following sequence parameters were used: single-shot gradient echo, echo time (TE): 26ms; repetition time (TR): 2500ms; flip angle: 82˚; spatial resolution: 1.45 x 1.8 x 1.45mm^3; field of view (FOV): 210 x 187.6 x 70.2mm; SENSE factor: 2.1; with 179 volumes per run). To facilitate post hoc physiological noise correction of the fMRI data, we recorded chest movement data using a respiratory bellow throughout the scans (sampling rate: 496Hz). A pulse oximeter was attached to the second digit of each participant's foot to record oxygen saturation and cardiac pulse. All physiological measurement devices were connected to a data acquisition device (Invivo; Phillips Medical Systems, Orlando, Florida) coupled with a desktop computer running the corresponding recording software.

For experiment 2, we centred 36 sagittal over the postcentral gyrus, with coverage over the thalamus and brainstem. The following sequence parameters were used: single-shot gradient echo, echo time (TE): 30ms; repetition time (TR): 2200ms; flip angle: 82˚; spatial resolution: 2.3mm^3; field of view (FOV): 210 x 210 x 82.8mm; SENSE factor: 2.1; with 167 volumes per run. We additionally acquired sagittal T2w structural images of patients' cervical spinal cord at the lesion level to quantify spared tissue bridges. These scans were acquired in a separate testing session using a 3 Tesla MAGNETOM Prisma Siemens Healthcare system (Erlangen, Germany) with a 64-channel head/neck coil. The sagittal T2w sequence was acquired using the following parameters: TR: 3500ms; TE=84ms; flip angle: 160; echo train length: 14; spatial resolution: 0.3x0.3x2.5mm; FOV 220mm x 220mm x 55mm.

2.5 MRI preprocessing and analysis

fMRI data preprocessing was applied to each individual fMRI run using FSL's Expert Analysis Tool FEAT (version 6.0; https://fsl.fmrib.ox.ac.uk/fsl/fslwiki/FEAT). To ensure consistent alignment of the hemisphere of interest in Experiment 1, we flipped the raw data along the x-axis for participants whose most impaired body side was the right side (or matched for controls). Similarly, in Experiment 2, we applied the same procedure for participants for whom the right side of the face was tested. This ensured that the hemisphere contralateral to the most impaired side of the body (in Experiment 1) or the tested face side (in Experiment 2) was consistently aligned.

Experiment 1

As experiment 1 was part of a larger study that focuses on brainstem imaging[35], we applied an optimised brainstem fMRI preprocessing pipeline based on previous research[42-46]. This pipeline included brain extraction using FSL's automated brain extraction tool (BET[47]), motion correction using FMRIB's Linear Image Registration Tool (MCFLIRT[48]), a 90s high-pass temporal filter implemented via FSL's Expert Analysis Tool (FEAT[49]), and spatial smoothing using a 3mm full-width-at-half-maximum (FWHM) isotropic Gaussian kernel. Further denoising was completed using FSL's Physiological Noise Modelling (PNM[50]). Cardiac and respiratory phases were assigned slicewise to each volume of the EPI image time series. The physiological noise regression model comprised a total of 34 regressors: 4th-order harmonics for both the cardiac and respiratory cycles, 2nd-order harmonics for their interactions, and individual regressors for heart rate and respiration volume. We visually inspected the waveforms to ensure accurate identification of the peaks of the cardiac and respiratory cycles, making adjustments as needed. The resulting voxelwise confound regressors were incorporated into the first-level general linear model (GLM).

Independent component analysis (ICA) was conducted using the Multivariate Exploratory Linear Optimized Decomposition interface (MELODIC[51]). The resulting components were classified as either "Noise" or "Signal" based on visual inspection of their spatial maps, time series, and power spectra information, following the guidelines published by Griffanti et al. [52]. Two independent researchers labelled the components to assess interrater reliability. Cohen's kappa indicated strong agreement between raters, with an estimated score of 0.85 (95% CI: 0.82 to 0.88). The ICA-derived noise regressors were subsequently added to the GLM design matrix.

First-level parameter estimates were computed using a voxel-based general linear model (GLM) based on the gamma hemodynamic response function and its temporal derivatives. Time series statistical analysis was conducted using FILM (FMRIB's Improved Linear Model) with local autocorrelation correction. Confound regressors were created for the hand movement tasks. Face movement was contrasted with rest. A fixed effects higher-level analysis was run for each participant to average across runs.

Experiment 2

Standard preprocessing steps were included for the experiment, including brain extraction using an automated brain extraction tool BET[47], motion correction using MCFLIRT[48], spatial smoothing using a 3mm full-width-at-half-maximum (FWHM) Gaussian kernel, and high-pass temporal filtering using a cut-off of 90s. First-level parameter estimates were computed using a voxel-based general linear model (GLM) based on the gamma hemodynamic response function and its temporal derivatives. Time series statistical analysis was conducted using FILM (FMRIB's Improved Linear Model) with local autocorrelation correction. To reduce

noise artefacts, scan-wise cerebrospinal fluid (CSF) and white matter time series were added to the model as nuisance regressors. Contrasts were defined for each face stimulation condition versus rest. A further regressor of no interest was defined for the 0.8s in which a visual cue was provided without tactile stimulation. A fixed effects higher-level analysis was run for each participant to average across runs.

2.5.1 MRI co-registration

We registered each participant's fMRI data to the T1-weighted image, using 6 degrees of freedom and the mutual information cost function, and then optimised using boundary-based registration (BBR[53]).

2.5.2 Region of interest definition

Face-to-hand area remapping was studied using anatomical regions of interest (ROIs) of S1 and the S1 hand area. As Brodmann area 3b of S1 has specifically been described to undergo drastic reorganisation in non-human primate models of SCI[5], we focused our analysis on this area (as defined by the atlas by Glasser et al. [54]). We further segmented this S1 ROI into 49 bands (Figure 1A) as in Schone et al. [55] to study the distribution of activity across this region.

We used an anatomical mask of the S1 hand area, as commonly used to investigate somatotopic hand representations and plasticity[56-60]. The S1 hand area ROI was defined by selecting the nodes approximately 1 cm below and above the anatomical hand knob within the S1 area 3b ROI (Figure 1C). We selected this conservative boundary of the hand ROI to be certain that our ROI did not expand into the S1 face area. The S1 hand area ROIs were first projected onto the individual participant's inflated cortical surface and then onto their 3D T1-weighted images. The cortical surface projections were constructed from each participant's T1-weighted images using FreeSurfer v6.0 (https://surfer.nmr.mgh.harvard.edu/)[61,62] and Connectome Workbench v1.3.2 (https://www.humanconnectome.org/software)[63].

2.5.3 Functional MRI analysis

Area 3b bands analysis

To investigate the distribution of face activity across S1, the statistical maps from the second-level analysis of experiments 1 and 2 were projected onto each participant's cortical surface using cortical-ribbon mapping and then onto the fs-LR surface template brain. We then extracted the peak activity (z-value) in each of the 49 S1 area 3b ROI bands.

Level of activity analysis

To explore univariate activity, we extracted the average z-value under the S1 hand area ROI contralateral to the most impaired body side during lip movement versus rest (experiment 1) or contralateral to the stimulated face side during forehead, lip, or chin stimulation versus rest (experiment 2).

Cortical distance analysis

To assess for a shift in face activity in SCI patients relative to controls, we extracted the peak vertex (i.e., maximally activated vertex on the FS-LR inflated surface) for each participant during lip movement (experiment 1) and for each of the stimulation conditions (experiment 2) within the S1 area 3b ROI. We then calculated the geodesic distance from an anchor placed in the S1 foot area (vertex 5550 on the fs-LR surface template brain) to the peak vertex for forehead, lip and chin stimulation.

Representational similarity analysis
To gain insights beyond the broad topographic distribution of the face representation, we employed multivariate representational similarity analysis (RSA). This method allows us to capture more subtle changes in the relationships between face-evoked activity patterns within the S1 hand area. Unlike traditional univariate analyses, RSA considers the full multidimensional activity pattern elicited by tactile stimulation of a body part, making it more sensitive to detecting underlying sensorimotor representations. We, therefore, calculated the dissimilarity between the activity patterns for each pair of face stimulation conditions within the S1 hand area.

We estimated the representational dissimilarity between face locations using the cross-validated squared Mahalanobis distance[64,65], adhering to previously established procedures[27,57,66,67]. We first extracted the voxel-wise parameter estimates (betas) and the model fit residuals under the ROI, then prewhitened the betas using the model fit residuals. Next, we calculated the cross-validated squared Mahalanobis distances between each pair of conditions, using the four runs as independent cross-validation folds. The resulting distances were averaged across the folds. The dissimilarity values for all pairs of conditions were initially assembled in a representational dissimilarity matrix (RDM), with a width and height corresponding to the number of conditions. To quantify the strength of the representation or "representational separability", we averaged the unique off-diagonal values of the RDM. Here, if conditions cannot be statistically differentiated (i.e. when a parameter is not represented in the ROI), the expected value of the distance estimate is 0. In contrast, if activity patterns can be distinguished, this value will be larger than 0.

2.5.4 Structural MRI analysis

Midsagittal tissue bridge analysis
We used sagittal T2w structural images of the cervical spinal cord at the lesion level to quantify spared tissue bridges[68-70]. The segmentation was performed using Jim 7.0 software (Xinapse Systems, Aldwincle, UK), which has demonstrated high intra- and interobserver reliability[69,70]. The experimenter conducting the manual segmentation was blinded to patient identity. Images from two patients were excluded due to metal artefacts or insufficient data quality, which would prevent reliable lesion quantification. Tissue bridges were defined as the relatively hypointense intramedullary region between the hyperintense CSF on one side and the cystic cavity on the other. We measured the smallest width of ventral and dorsal tissue bridges on the midsagittal slice and summed them to obtain the total width of the remaining tissue bridges.

2.6 Statistical analysis
We carried out statistical analysis using JASP (v0.17.2.1). We used standard approaches for statistical analysis, as mentioned in the Results section. Outliers were defined as values that were more than 3 standard deviations greater or lower than the group mean and were replaced with group-specific averages.

If normality was violated (assessed using the Shapiro-Wilk test), appropriate non-parametric statistical testing was used. Given our strong hypothesis based on previous literature, all group testing was one-tailed. We corrected for multiple corrections per reorganisation measure in our group comparisons using the Bonferroni correction. Uncorrected p-values are reported with the adjusted alpha-levels. Given the exploratory nature of our correlational analysis, no correction for multiple comparisons was carried out here.

Bayesian analysis was conducted for the main comparisons to investigate support for the null hypothesis with the Cauchy prior width set at 0.707 (i.e., JASP's default). If assumptions of normality were violated, we ran group comparisons using Mann Whitney Bayesian testing with 1000 permutations. Following the conventional cut-offs, a Bayes Factor (BF) smaller than 1/3 is considered substantial evidence in favour of the null hypothesis. A BF greater than 3 is considered substantial evidence and a BF greater than 10 is considered strong evidence in favour of the alternative hypothesis. A BF between 1/3 and 3 is considered weak or anecdotal evidence[71,72].

For the Area 3b bands analysis, comparisons were made between SCI patient and control data for each band using non-parametric permutation t-tests in the SPM1D Matlab toolbox for one-dimensional data (SPM1D M.0.4.12; https://spm1d.org/). SPM1D utilises random field theory (RFT) to make statistical inferences on one-dimensional data by treating discrete data points, such as individual bands, as part of a continuous field. This approach accounts for spatial correlations in the data and estimates the probability of observing a supra-threshold test statistic under the null hypothesis.

3. Results

Experiment 1: Investigating face-to-hand area remapping using a movement paradigm

In Experiment 1, we aimed to replicate the procedures from previous studies using a lip movement paradigm to investigate face-to-hand area remapping in S1 area 3b. First, we visualised the distribution of lip movement activity along S1 by extracting the peak lip movement activity in each of our S1 bands (Figure 1A-B). Consistent with the somatotopic organisation of the somatosensory homunculus, we saw the highest lip movement activity in the lateral bands of S1 and lower activity in the medial bands of S1[28,73]. Notably, we did not find a greater distribution of face activity across these bands in SCI patients compared to control participants (non-parametric permutation t-tests*;* largest Z= -2.32, $P = 0.25$; smallest Z < 0.00, $P > 0.99$**)**.

We further hypothesised that face-to-hand area remapping in cervical SCI patients would result in increased activity in the S1 hand area (Figure 1C) during lip movements. However, no such increase was observed compared to controls (t(34)=0.46, p = 0.68; BF10 = 0.24; Figure 1D). Crucially, if the lip representation shifted towards but did not invade the S1 hand area, then it is possible that no changes in lip movement activity levels would be observed in the S1 hand area, but rather, there would be a smaller geodesic distance between peak lip activity and an anchor placed in the S1 foot area. However, no significant difference in lip-to-anchor distance between SCI patients and controls was found (W = 154, p = 0.58; BF = 0.34; Figure 1B).

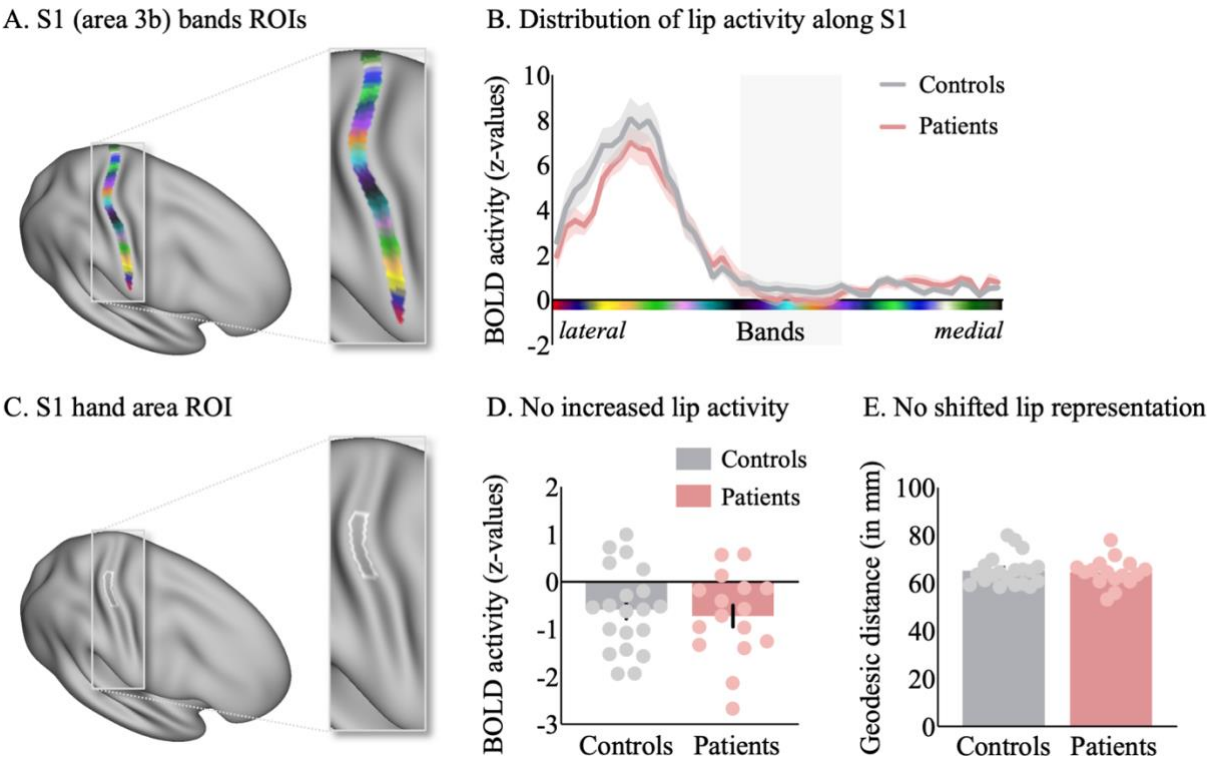

Figure 1: No evidence in favour of face-to-hand area remapping using a lip movement paradigm. A) S1 (area 3b) region of interest (ROI) divided into 49 distinct bands. B) Lip movement successfully activated S1 in both controls (grey) and patients (red). Shared areas represent the standard error of the mean. Peak activity during lip movement was highest in the lateral S1 bands. The grey shaded bands represent the bands that overlap with the S1 hand area ROI in C). D) There was no increased lip movement activity in the S1 hand area of patients (red) compared to controls (grey). Dots represent individual participants. Error bars represent the standard error of the mean. E) We calculated the geodesic distance in mm for each participant between an anchor in the S1 foot area and peak lip movement activity. We did not find a shorter lip-to-anchor distance in patients compared to controls, indicating that there is no shifted lip movement representation following cervical spinal cord injury.

Experiment 2: Investigating face-to-hand area remapping using a tactile stimulation paradigm

In experiment 2, we used a tactile face stimulation paradigm to closely match procedures that have been used in classical non-human primate studies. Furthermore, since the lip representation does not neighbour the hand representation in humans, we expanded our investigation to include the forehead, lips, and chin, ensuring that each skin area innervated by the distinct trigeminal nerve branches was represented in our investigation (Figure 2A). We found that our custom-built device, based on soft pneumatic actuator (SPA) technology, effectively activated S1 (Figure 2B-D). A qualitative inspection of the distribution of peak activity along S1 showed that while lip and chin stimulation predominantly activated S1 lateral of the S1 hand area, forehead stimulation appeared to be represented both lateral and medial to the S1 hand area. Importantly, we did not find a greater distribution of face activity across these bands in SCI patients compared to control participants for the forehead (largest Z= -1.48, P = 0.64; smallest Z < 0.00, P > 0.99**)**, lip (largest Z= -1.64, P = 0.52; smallest Z = 0.02, P > 0.99**)**, or chin stimulation (largest Z= -1.98, P = 0.36; smallest Z < 0.00, P > 0.99**)**.

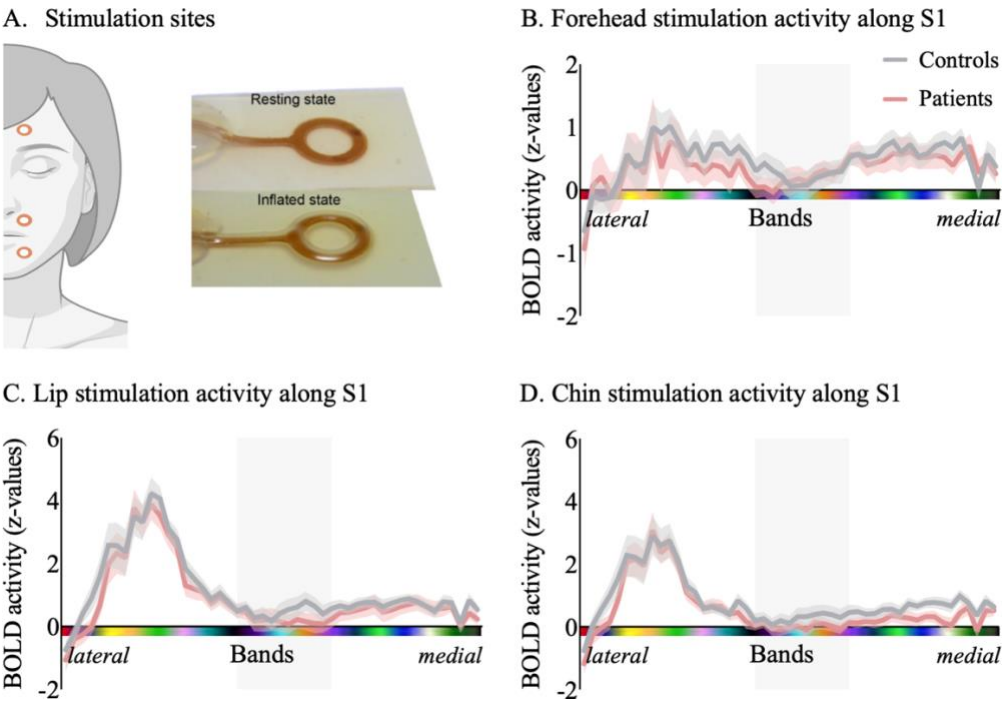

Figure 2: Tactile face stimulation successfully activated S1. A) We applied vibrotactile stimulation to the forehead, lips, and chin using a custom-built device based on soft pneumatic actuator (SPA) technology to study face-to-hand area reorganisation in S1. Peak activity along the S1 area 3b band ROIs during stimulation of the forehead (B), lips (C) and chin (D). While peak activity was most predominant in the lateral bands of S1 for lip and chin stimulation, forehead activity appears to be represented both lateral and medial to the S1 hand area. The grey shaded areas represent the bands that overlap with the S1 hand area. Annotations are as in Figure 1.

As in Experiment 1, we hypothesised that if face-to-hand area remapping had occurred in cervical SCI patients, we would observe increased activity in the S1 hand area (Figure 3A) and/or a medial shift in peak activity (Figure 3B) in patients compared to controls during forehead, lip, or chin stimulation. However, we did not find increased S1 hand area activity in SCI patients compared to controls during stimulation of the forehead ($W = 194$, $p = 0.79$; $BF_{10} = 0.23$; adjusted $\alpha = 0.017$), lips ($t_{(35)} = 0.47$, $p = 0.68$; $BF_{10} = 0.24$), or chin ($W = 193$, $p = 0.78$; $BF_{10} = 0.21$). We similarly did not observe a significant medial shift in peak activity during forehead ($W = 127.5$, $p = 0.90$, $BF_{10} = 0.17$; adjusted $\alpha = 0.017$), lips ($W = 140.5$, $p = 0.81$, $BF_{10} = 0.67$), or chin stimulation ($W = 123.5$, $p = 0.92$, $BF_{10} = 0.14$) in patients compared to controls. Note that similar results were observed when the geodesic analysis was restricted to the S1 hand area and the adjacent inferior S1 region (i.e., S1 face area; forehead: ($t_{(35)} = -0.94$, $p = 0.82$; $BF_{10} = 0.19$; adjusted $\alpha = 0.017$; lip: $W = 134.5$, $p = 0.85$, $BF_{10} = 0.18$; chin: $W = 129.5$, $p = 0.88$, $BF_{10} = 0.18$).

Next, we used multivariate representational similarity analysis (RSA) to gain insights into the underlying activity pattern elicited by tactile stimulation of the face. We hypothesised that if reorganisation had occurred, there would be more distinct information in the S1 hand area, allowing for better differentiation between the face conditions. In other words, the average representational separability (or 'representation strength') between the activity patterns elicited by stimulating different face parts would be higher. First, we visualised the separability, measured as the mean inter-face parts distance, across each of our S1 bands for both the SCI patients and controls (Figure 3C). We saw greater representational separability in the bands

lateral and medial to the S1 hand area, with no difference in separability scores between the SCI patient and control groups (largest Z= 2.28, $P = 0.40$; smallest Z = 0.08, $P > 0.99$**)**. A comparison of face-part separability within the S1 hand area revealed a trend towards greater representational separability in cervical SCI patients compared to controls (Figure 3D; W = 123, p = 0.09; BF_{10} = 0.94), with the Bayes factor showing anecdotal results in favour of the null hypothesis.

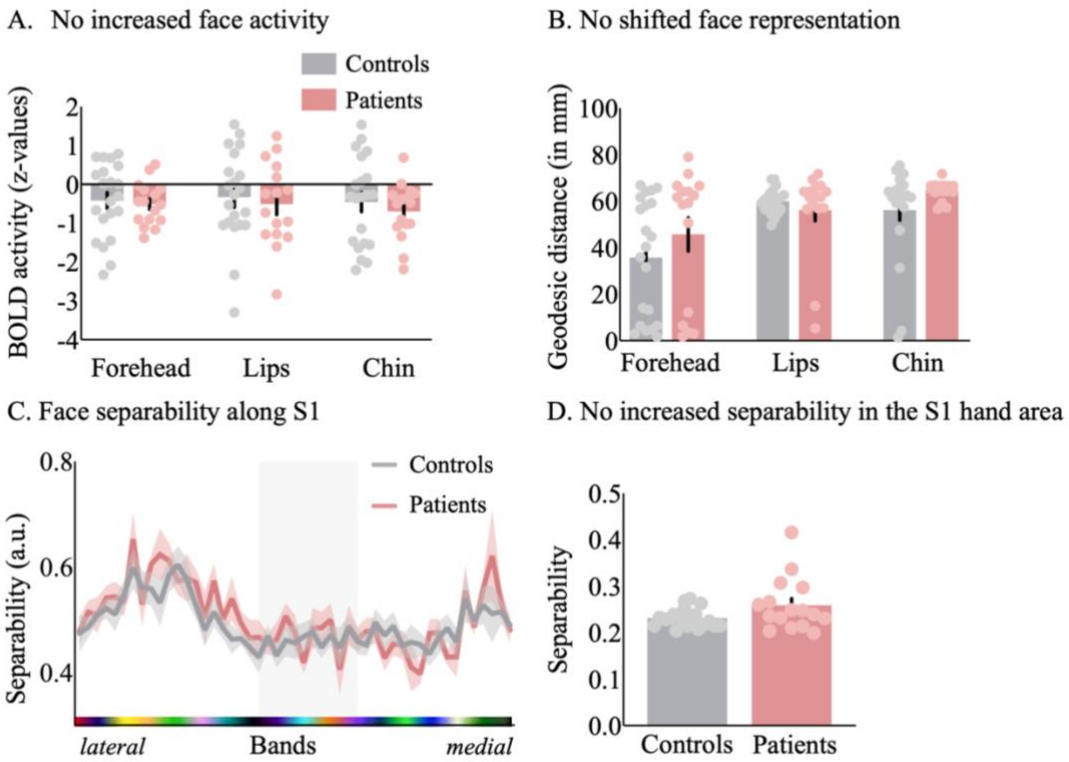

Figure 3: A tactile stimulation paradigm did not show evidence in favour of face-to-hand area reorganisation in S1. A) There was no increased average face activity in the S1 hand area of patients compared to controls during forehead, lip or chin stimulation. B) We calculated the geodesic distance in mm for each participant between an anchor in the S1 foot area and peak activity for each of our stimulation conditions. We did not find any significant differences between patients and controls for any of the conditions, indicating that there was no shifted forehead, lip, or chin representation in patients compared to controls. C) Mean face-part separability scores along the S1 area 3b band ROIs. The grey shaded areas represent the bands that overlap with the S1 hand area. D) A comparison of face-part separability within the S1 hand area did not reveal significant differences between patients and controls. Annotations are as in Figure 2.

Clinical correlates of face-to-hand remapping

Next, we aimed to understand which clinical, behavioural, and structural spinal cord determinants may drive face-to-hand area remapping in S1 of cervical SCI patients. Given that we assume the representational similarity analysis is the most sensitive in detecting reorganisation, we focused our correlational analysis on our outcome measure of face-to-face part representational separability in the S1 hand area (Figure 4). We found that the number of years since SCI showed a trend towards a negative correlation with our measure of face-to-hand area interface distances (r_s = –0.48, p=0.06), suggesting that face representations may

become less distinct over years since SCI. We did not find any significant correlations with the retained sensorimotor function of the upper limbs (GRASSP; $r_s = 0.74$, $p = 0.09$), pain ($r_s = 0.01$, $p = 0.98$), or spared midsagittal spinal tissue bridges at the lesion level ($r_s = 0.19$, $p = 0.54$).

Preservation of the S1 hand representation may interfere with S1 face-to-hand area remapping. We, therefore, explored whether SCI patients with more salient hand representation in the S1 hand area exhibit less face-to-hand area remapping. A subset of patients from this study (n = 9) also participated in our previous study, where we examined preserved finger somatotopy in cervical SCI patients[57]. We extracted the somatotopic hand representation typicality (or normality) for each of these patients from our previous study. However, we did not find a significant correlation (-0.37, p = 0.33), suggesting that the preservation of the S1 hand representation does not influence potential face-to-hand area remapping.

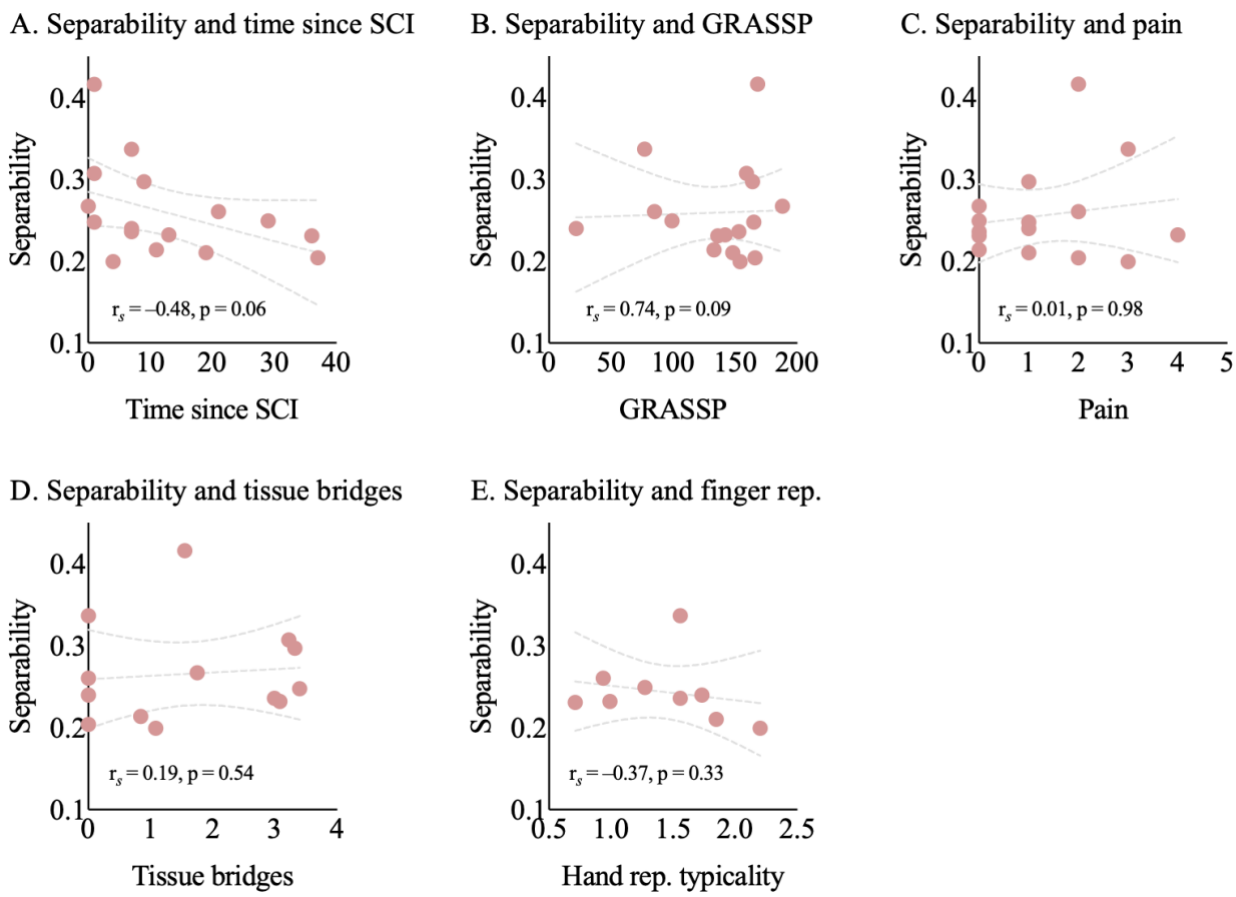

Figure 4: No significant correlations between face-to-hand area remapping and clinical, behavioural, and structural spinal cord measures. We examined clinical, behavioural, and spinal cord structural correlates for face-to-hand area remapping, quantified using mean face-part representational separability in the S1 hand area. A) There was a trend towards a significant correlation between representational separability and time since SCI. There was no significant correlation between representational separability and sensorimotor function of the upper limbs as measured using the GRASSP (B), pain (C), and spared midsagittal spinal tissue bridges at the lesion level (D). E) Finally, we found that preservation of the S1 hand representation does not significantly correlate with S1 face-to-hand area remapping. Rep. = representation. Annotations are as in Figure 2.

4. Discussion

In this study, we aimed to resolve inconsistencies in the reorganisation literature and assess face-to-hand area remapping in human cervical SCI patients in unprecedented detail. To do so, we utilised both movement (experiment 1) and vibrotactile stimulation paradigms (experiment 2), allowing us to investigate the full architecture of S1 face reorganisation. We found no significant evidence of changes in face representations following SCI compared to control participants across three distinct reorganisation measures. Furthermore, we found no significant correlations between face-to-hand area reorganisation and the clinical, behavioural, and structural outcome measures. Given the comprehensive scope of our investigation, we suggest that S1 face-to-hand area remapping is not apparent after cervical SCI in humans.

Most prior human research into cortical reorganisation following SCI has focused exclusively on the lower face, primarily the mouth. Instead, our study considered multiple parts of the face, systematically assessing each of the distinct facial areas innervated by trigeminal nerve branches. Our findings provide evidence in favour of stable face representations, with no significant evidence showing remapping of either the upper or lower face areas into the deprived hand region. This adds to the growing body of literature demonstrating stable sensorimotor representations in humans following sensory deprivation[27,55-57,60,67,74-77]. These preserved representations can be utilised to restore sensorimotor functions through brain-computer interfaces. For instance, through intracortical microstimulation in the S1 hand area, researchers have been able to elicit fine-grained tactile sensations within the hand of cervical SCI patients several years after their injury[74,78-80].

Yet, how can such contrasting accounts of stability and reorganisation coexist in the literature? Through a homeostatic plasticity model, Muret and Makin [81] propose that body-part representations are more broadly distributed across the homunculus than previously believed. Upon sensory deprivation, these underlying body-part representations are unmasked, which may be misinterpreted as reorganisation. Our finding of two distinct peaks for face-part separability and forehead activation, alongside similar evidence from others[82,83], supports the notion of distributed body-part representations across the sensorimotor cortices. Critically, a limitation of previous reorganisation research, in both animals and humans, is that cortical maps are often defined using a winner-take-all approach[60,77]. Through this approach, any underlying representational overlap between body parts is disregarded, with the boundaries of cortical areas defined according to the dominant body-part response. Therefore, in the absence of hand activity following an SCI, the native S1 hand area may be reassigned to the next dominant body part included in the analysis, i.e. the face, and subsequently misinterpreted as evidence for cortical reorganisation. Indeed, while Jain, Qi, Collins and Kaas [6] reported large-scale functional reorganisation in non-human primate models of SCI, they simultaneously found anatomical evidence against reorganisation, showing that the myelin boundaries between the hand and face areas remain stable. In the present study, we addressed this methodological confound by avoiding winner-take-all approaches and employing RSA to account for the potential overlap of underlying representations.

Through RSA, we were able to investigate not only whether new information content emerges in the deprived cortex but also how this information is structured. This analysis revealed a trend towards greater face-part separability within the S1 hand area in cervical SCI patients compared to the controls, suggesting that the representation of the face may be more distinct in the patients. However, we also observed a trend of decreasing face-part separability as the time since injury increased. Given the lack of significant effects, these results should be interpreted

with caution. Nevertheless, a decrease in face-part separability within the S1 hand area over time is consistent with previous literature demonstrating reduced sensorimotor activation in SCI patients as time since injury increases[57,84]. It is possible that there is a general loss of representations in the deprived cortex of SCI patients due to disuse in everyday life. Yet, we found no further correlates of face-part separability. Note that the reduced sample sizes for the correlations conducted against spared midsagittal tissue bridges (n = 13) and preserved hand representation typicality scores (n = 9) reduced the power to find a significant relationship in these analyses.

While we attempted to account for key methodological differences between reorganisation research using animal models of SCI and human SCI patients, there were some methodological differences we could not overcome. Fundamentally, animal studies typically model SCI via uni- or bilateral transection of the ascending dorsal column[3,5,6,85,86]. In contrast, human SCI typically arises from a traumatic incident, leading to a pattern of disruption that is more anatomically and clinically heterogeneous and often resulting in both sensory and motor impairments with a range of completeness. Furthermore, in the current study, we used fMRI, which indirectly measures thousands of neurons within a single voxel, whereas invasive electrophysiological recordings utilised in animal models are capable of detecting neural activity at a single-neuron resolution. Despite this limited resolution, previous fMRI studies in non-human primate models of SCI have been able to demonstrate reorganisation[87-89]. Moreover, fine-grained intracortical stimulation of the deprived S1 hand area in human cervical SCI patients has been shown to only elicit sensations within the paralysed hand and not in adjacent body parts, such as the face. Therefore, it is unlikely that these methodological discrepancies solely account for the absence of face-to-hand remapping in our human SCI cohort.

Importantly, while our findings do not demonstrate face-to-hand remapping in human SCI patients, this does not imply that reorganisation may never occur in humans. Reorganisation has been documented in other contexts, such as congenital limb loss[27,90-93]. Yet, emerging evidence suggests that this reorganisation is restricted to the prenatal or early developmental stages[27,55,90,91,94]. A recent longitudinal study by Schone et al. [55] demonstrated that the adult human brain is remarkably stable. Specifically, the researchers tested individuals before and after arm amputation and showed that somatosensory representations of the face and missing arm remained unaltered[55]. Thus, while non-human primate research suggests that the somatosensory system of adult mammals remains highly plastic[6,9,24,95], it is possible that the temporal limits of cortical reorganisation in humans differ.

Together, our findings call for the assumption of large-scale face-to-hand remapping in human SCI patients to be revisited. Specifically, our results emphasise the need to critically reassess the translation of findings from animal models to humans. Further research is necessary to uncover the specific conditions under which cortical remapping may occur in humans and better understand its potential role in recovery following SCI.

Data availability
Aggregated data will be made available online upon publication.

Acknowledgements
We thank the participants for their participation in the study, Sijamini Baskaralingam and Ingrid Odermatt for their help with data collection, Roger Luchinger and the Institute for Biomedical Imaging for scanning support, and Hunter Schone for his expert support in fMRI data analysis.

Funding support
P. Howell and S. Kikkert were supported by the Swiss National Science Foundation Ambizione Grant (PZ00P3_208996) and an ETH Career Seed Award. NW was supported by the Swiss National Science Foundation Grant 32003B_207719 and by the National Research Foundation, Prime Minister's Office, Singapore, under its Campus for Research Excellence and Technological Enterprise (CREATE) program (FHT). HS and JP were supported by the Swiss National Science Foundation and École polytechnique fédérale de Lausanne. PF was supported by the Swiss National Science Foundation Grant 32003B_204934. SSS was supported by a national MD-PhD scholarship from the Swiss National Science Foundation (323530_207038).

Competing interests
The authors declare that no current competing interests exist.

References

1. McDonald JW, Sadowsky C. Spinal-cord injury. *The Lancet*. 2002;359(9304):417-425. doi:10.1016/S0140-6736(02)07603-1
2. Jain N, Florence SL, Kaas JH. Reorganization of Somatosensory Cortex After Nerve and Spinal Cord Injury. *Physiology*. 1998;13(3):143-149. doi:10.1152/physiologyonline.1998.13.3.143
3. Kaas JH, Qi HX, Burish MJ, Gharbawie OA, Onifer SM, Massey JM. Cortical and subcortical plasticity in the brains of humans, primates, and rats after damage to sensory afferents in the dorsal columns of the spinal cord. *Exp Neurol*. Feb 2008;209(2):407-16. doi:10.1016/j.expneurol.2007.06.014
4. Jain N, Catania KC, Kaas JH. Deactivation and reactivation of somatosensory cortex after dorsal spinal cord injury. *Nature*. 1997;386(6624):495-498.
5. Reed JL, Liao CC, Qi HX, Kaas JH. Plasticity and Recovery After Dorsal Column Spinal Cord Injury in Nonhuman Primates. *J Exp Neurosci*. 2016;10(Suppl 1):11-21. doi:10.4137/jen.S40197
6. Jain N, Qi HX, Collins CE, Kaas JH. Large-scale reorganization in the somatosensory cortex and thalamus after sensory loss in macaque monkeys. *J Neurosci*. Oct 22 2008;28(43):11042-60. doi:10.1523/jneurosci.2334-08.2008
7. Kambi N, Halder P, Rajan R*, et al*. Large-scale reorganization of the somatosensory cortex following spinal cord injuries is due to brainstem plasticity. *Nature Communications*. 2014/04/08 2014;5(1):3602. doi:10.1038/ncomms4602
8. Ghosh A, Sydekum E, Haiss F*, et al*. Functional and Anatomical Reorganization of the Sensory-Motor Cortex after Incomplete Spinal Cord Injury in Adult Rats. *The Journal of Neuroscience*. 2009;29(39):12210-12219. doi:10.1523/jneurosci.1828-09.2009
9. Merzenich MM, Kaas JH, Wall J, Nelson RJ, Sur M, Felleman D. Topographic reorganization of somatosensory cortical areas 3b and 1 in adult monkeys following restricted deafferentation. *Neuroscience*. Jan 1983;8(1):33-55. doi:10.1016/0306-4522(83)90024-6
10. Melo MC, Macedo DR, Soares AB. Divergent Findings in Brain Reorganization After Spinal Cord Injury: A Review. *Journal of Neuroimaging*. 2020;30(4):410-427. doi:https://doi.org/10.1111/jon.12711
11. Bruehlmeier M, Dietz V, Leenders KL, Roelcke U, Missimer J, Curt A. How does the human brain deal with a spinal cord injury? *Eur J Neurosci*. Dec 1998;10(12):3918-22. doi:10.1046/j.1460-9568.1998.00454.x
12. Corbetta M, Burton H, Sinclair RJ, Conturo TE, Akbudak E, McDonald JW. Functional reorganization and stability of somatosensory-motor cortical topography in a tetraplegic subject with late recovery. *Proc Natl Acad Sci U S A*. Dec 24 2002;99(26):17066-71. doi:10.1073/pnas.262669099
13. Freund P, Weiskopf N, Ward NS*, et al*. Disability, atrophy and cortical reorganization following spinal cord injury. *Brain*. Jun 2011;134(Pt 6):1610-22. doi:10.1093/brain/awr093
14. Moore CI, Stern CE, Dunbar C, Kostyk SK, Gehi A, Corkin S. Referred phantom sensations and cortical reorganization after spinal cord injury in humans. *Proc Natl Acad Sci U S A*. Dec 19 2000;97(26):14703-8. doi:10.1073/pnas.250348997

15. Perani D, Brunelli GA, Tettamanti M*, et al*. Remodelling of sensorimotor maps in paraplegia: a functional magnetic resonance imaging study after a surgical nerve transfer. *Neuroscience Letters*. 2001/04/27/ 2001;303(1):62-66. doi:https://doi.org/10.1016/S0304-3940(01)01649-4
16. Henderson LA, Gustin SM, Macey PM, Wrigley PJ, Siddall PJ. Functional reorganization of the brain in humans following spinal cord injury: evidence for underlying changes in cortical anatomy. *J Neurosci*. Feb 16 2011;31(7):2630-7. doi:10.1523/jneurosci.2717-10.2011
17. Turner JA, Lee JS, Schandler SL, Cohen MJ. An fMRI investigation of hand representation in paraplegic humans. *Neurorehabil Neural Repair*. Mar 2003;17(1):37-47. doi:10.1177/0888439002250443
18. Wrigley PJ, Press SR, Gustin SM*, et al*. Neuropathic pain and primary somatosensory cortex reorganization following spinal cord injury. *Pain*. Jan 2009;141(1-2):52-9. doi:10.1016/j.pain.2008.10.007
19. Kandel ER. *Principles of Neural Science, Fifth Edition*. McGraw-Hill Education; 2013.
20. Moxon KA, Oliviero A, Aguilar J, Foffani G. Cortical reorganization after spinal cord injury: Always for good? *Neuroscience*. 2014/12/26/ 2014;283:78-94. doi:https://doi.org/10.1016/j.neuroscience.2014.06.056
21. Jutzeler CR, Curt A, Kramer JL. Relationship between chronic pain and brain reorganization after deafferentation: A systematic review of functional MRI findings. *Neuroimage Clin*. 2015;9:599-606. doi:10.1016/j.nicl.2015.09.018
22. Zaaimi B, Edgley SA, Soteropoulos DS, Baker SN. Changes in descending motor pathway connectivity after corticospinal tract lesion in macaque monkey. *Brain*. Jul 2012;135(Pt 7):2277-89. doi:10.1093/brain/aws115
23. Zörner B, Bachmann LC, Filli L*, et al*. Chasing central nervous system plasticity: the brainstem's contribution to locomotor recovery in rats with spinal cord injury. *Brain*. Jun 2014;137(Pt 6):1716-32. doi:10.1093/brain/awu078
24. Pons TP, Garraghty PE, Ommaya AK, Kaas JH, Taub E, Mishkin M. Massive Cortical Reorganization After Sensory Deafferentation in Adult Macaques. *Science*. 1991;252(5014):1857-1860. doi:doi:10.1126/science.1843843
25. Kaas JH. What, if anything, is SI? Organization of first somatosensory area of cortex. *Physiol Rev*. Jan 1983;63(1):206-31. doi:10.1152/physrev.1983.63.1.206
26. Kikkert S, Sonar HA, Freund P, Paik J, Wenderoth N. Hand and face somatotopy shown using MRI-safe vibrotactile stimulation with a novel soft pneumatic actuator (SPA)-skin interface. *NeuroImage*. 2023;269:119932.
27. Root V, Muret D, Arribas M*, et al*. Complex pattern of facial remapping in somatosensory cortex following congenital but not acquired hand loss. *eLife*. 2022/12/30 2022;11:e76158. doi:10.7554/eLife.76158
28. Penfield W, Boldrey E. SOMATIC MOTOR AND SENSORY REPRESENTATION IN THE CEREBRAL CORTEX OF MAN AS STUDIED BY ELECTRICAL STIMULATION1. *Brain*. 1937;60(4):389-443. doi:10.1093/brain/60.4.389
29. Curt A, Alkadhi H, Crelier GR, Boendermaker SH, Hepp-Reymond MC, Kollias SS. Changes of non-affected upper limb cortical representation in paraplegic patients as assessed by fMRI. *Brain*. Nov 2002;125(Pt 11):2567-78. doi:10.1093/brain/awf250

30. Lotze M, Laubis-Herrmann U, Topka H, Erb M, Grodd W. Reorganization in the primary motor cortex after spinal cord injury - A functional Magnetic Resonance (fMRI) study. *Restor Neurol Neurosci*. 1999;14(2-3):183-187.
31. Mikulis DJ, Jurkiewicz MT, McIlroy WE*, et al*. Adaptation in the motor cortex following cervical spinal cord injury. *Neurology*. Mar 12 2002;58(5):794-801. doi:10.1212/wnl.58.5.794
32. Turner JA, Lee JS, Martinez O, Medlin AL, Schandler SL, Cohen MJ. Somatotopy of the motor cortex after long-term spinal cord injury or amputation. *IEEE Trans Neural Syst Rehabil Eng*. Jun 2001;9(2):154-60. doi:10.1109/7333.928575
33. Oligschläger S, Huntenburg JM, Golchert J, Lauckner ME, Bonnen T, Margulies DS. Gradients of connectivity distance are anchored in primary cortex. *Brain Structure and Function*. 2017/07/01 2017;222(5):2173-2182. doi:10.1007/s00429-016-1333-7
34. Kalsi-Ryan S, Beaton D, Curt A*, et al*. The Graded Redefined Assessment of Strength Sensibility and Prehension: reliability and validity. *J Neurotrauma*. Mar 20 2012;29(5):905-14. doi:10.1089/neu.2010.1504
35. Howell P, Odermatt I, Harrison O*, et al*. Distinguishing the activity of adjacent somatosensory nuclei within the brainstem using 3T fMRI. *bioRxiv*. 2024:2024.11.27.625699. doi:10.1101/2024.11.27.625699
36. Sonar HA, Paik J. Soft Pneumatic Actuator Skin with Piezoelectric Sensors for Vibrotactile Feedback. Original Research. *Frontiers in Robotics and AI*. 2016-January-11 2016;2doi:10.3389/frobt.2015.00038
37. Sonar HA, Gerratt AP, Lacour SP, Paik J. Closed-Loop Haptic Feedback Control Using a Self-Sensing Soft Pneumatic Actuator Skin. *Soft Robotics*. 2020/02/01 2019;7(1):22-29. doi:10.1089/soro.2019.0013
38. Joshi S, Sonar H, Paik J. Flow Path Optimization for Soft Pneumatic Actuators: Towards Optimal Performance and Portability. *IEEE Robotics and Automation Letters*. 2021;6(4):7949-7956. doi:10.1109/LRA.2021.3100626
39. Corniani G, Saal HP. Tactile innervation densities across the whole body. *J Neurophysiol*. Oct 1 2020;124(4):1229-1240. doi:10.1152/jn.00313.2020
40. Sonar HA, Huang J-L, Paik J. Soft Touch using Soft Pneumatic Actuator–Skin as a Wearable Haptic Feedback Device. *Advanced Intelligent Systems*. 2021;3(3):2000168. doi:https://doi.org/10.1002/aisy.202000168
41. Choi S, Kuchenbecker KJ. Vibrotactile Display: Perception, Technology, and Applications. *Proceedings of the IEEE*. 2013;101(9):2093-2104. doi:10.1109/JPROC.2012.2221071
42. Meissner SN, Bächinger M, Kikkert S*, et al*. Self-regulating arousal via pupil-based biofeedback. *Nature Human Behaviour*. 2024/01/01 2024;8(1):43-62. doi:10.1038/s41562-023-01729-z
43. Faull OK, Jenkinson M, Clare S, Pattinson KT. Functional subdivision of the human periaqueductal grey in respiratory control using 7 tesla fMRI. *Neuroimage*. Jun 2015;113:356-64. doi:10.1016/j.neuroimage.2015.02.026
44. Beissner F, Deichmann R, Baudrexel S. fMRI of the brainstem using dual-echo EPI. *NeuroImage*. 2011/04/15/ 2011;55(4):1593-1599. doi:https://doi.org/10.1016/j.neuroimage.2011.01.042
45. Beissner F. Functional MRI of the Brainstem: Common Problems and their Solutions. *Clin Neuroradiol*. Oct 2015;25 Suppl 2:251-7. doi:10.1007/s00062-015-0404-0

46. Matt E, Fischmeister FPS, Amini A*, et al*. Improving sensitivity, specificity, and reproducibility of individual brainstem activation. *Brain Struct Funct*. Nov 2019;224(8):2823-2838. doi:10.1007/s00429-019-01936-3
47. Smith SM. Fast robust automated brain extraction. *Hum Brain Mapp*. Nov 2002;17(3):143-55. doi:10.1002/hbm.10062
48. Jenkinson M, Bannister P, Brady M, Smith S. Improved optimization for the robust and accurate linear registration and motion correction of brain images. *Neuroimage*. Oct 2002;17(2):825-41. doi:10.1016/s1053-8119(02)91132-8
49. Woolrich MW, Ripley BD, Brady M, Smith SM. Temporal Autocorrelation in Univariate Linear Modeling of FMRI Data. *NeuroImage*. 2001/12/01/ 2001;14(6):1370-1386. doi:https://doi.org/10.1006/nimg.2001.0931
50. Brooks JC, Beckmann CF, Miller KL*, et al*. Physiological noise modelling for spinal functional magnetic resonance imaging studies. *Neuroimage*. Jan 15 2008;39(2):680-92. doi:10.1016/j.neuroimage.2007.09.018
51. Smith SM, Jenkinson M, Woolrich MW*, et al*. Advances in functional and structural MR image analysis and implementat. *Neuroimage*. 2004;23 Suppl 1:S208-19. doi:10.1016/j.neuroimage.2004.07.051
52. Griffanti L, Douaud G, Bijsterbosch J*, et al*. Hand classification of fMRI ICA noise components. *Neuroimage*. Jul 1 2017;154:188-205. doi:10.1016/j.neuroimage.2016.12.036
53. Greve DN, Fischl B. Accurate and robust brain image alignment using boundary-based registration. *Neuroimage*. Oct 15 2009;48(1):63-72. doi:10.1016/j.neuroimage.2009.06.060
54. Glasser MF, Coalson TS, Robinson EC*, et al*. A multi-modal parcellation of human cerebral cortex. *Nature*. 2016/08/01 2016;536(7615):171-178. doi:10.1038/nature18933
55. Schone HR, Maimon Mor RO, Kollamkulam M*, et al*. Stable Cortical Body Maps Before and After Arm Amputation. *bioRxiv*. Dec 14 2023;doi:10.1101/2023.12.13.571314
56. Kikkert S, Kolasinski J, Jbabdi S*, et al*. Revealing the neural fingerprints of a missing hand. *Elife*. 2016;5:e15292.
57. Kikkert S, Pfyffer D, Verling M, Freund P, Wenderoth N. Finger somatotopy is preserved after tetraplegia but deteriorates over time. *Elife*. 2021;10:e67713.
58. Kolasinski J, Makin TR, Logan JP*, et al*. Perceptually relevant remapping of human somatotopy in 24 hours. *eLife*. 2016/12/30 2016;5:e17280. doi:10.7554/eLife.17280
59. Beukema P, Diedrichsen J, Verstynen TD. Binding During Sequence Learning Does Not Alter Cortical Representations of Individual Actions. *The Journal of Neuroscience*. 2019;39(35):6968-6977. doi:10.1523/jneurosci.2669-18.2019
60. Wesselink DB, Sanders ZB, Edmondson LR*, et al*. Malleability of the cortical hand map following a finger nerve block. *Sci Adv*. Apr 22 2022;8(16):eabk2393. doi:10.1126/sciadv.abk2393
61. Fischl B, Liu A, Dale AM. Automated manifold surgery: constructing geometrically accurate and topologically correct models of the human cerebral cortex. *IEEE Trans Med Imaging*. Jan 2001;20(1):70-80. doi:10.1109/42.906426
62. Dale AM, Fischl B, Sereno MI. Cortical surface-based analysis. I. Segmentation and surface reconstruction. *Neuroimage*. Feb 1999;9(2):179-94. doi:10.1006/nimg.1998.0395

63. Marcus DS, Harwell J, Olsen T*, et al*. Informatics and data mining tools and strategies for the human connectome project. *Front Neuroinform*. 2011;5:4. doi:10.3389/fninf.2011.00004
64. Nili H, Wingfield C, Walther A, Su L, Marslen-Wilson W, Kriegeskorte N. A Toolbox for Representational Similarity Analysis. *PLOS Computational Biology*. 2014;10(4):e1003553. doi:10.1371/journal.pcbi.1003553
65. *rsatoolbox, version 20fbe05*. Version 20fbe05. Github; 2017. https://github.com/ronimaimon/rsatoolbox
66. Odermatt IA, Schulthess-Lutz M, Mihelj E*, et al*. TMS-based neurofeedback training of mental finger individuation induces neuroplastic changes in the sensorimotor cortex. *bioRxiv*. 2024:2024.05.16.594100. doi:10.1101/2024.05.16.594100
67. Wesselink DB, van den Heiligenberg FMZ, Ejaz N*, et al*. Obtaining and maintaining cortical hand representation as evidenced from acquired and congenital handlessness. *eLife*. 2019/02/05 2019;8:e37227. doi:10.7554/eLife.37227
68. Vallotton K, Huber E, Sutter R, Curt A, Hupp M, Freund P. Width and neurophysiologic properties of tissue bridges predict recovery after cervical injury. *Neurology*. Jun 11 2019;92(24):e2793-e2802. doi:10.1212/wnl.0000000000007642
69. Huber E, Lachappelle P, Sutter R, Curt A, Freund P. Are midsagittal tissue bridges predictive of outcome after cervical spinal cord injury? *Ann Neurol*. May 2017;81(5):740-748. doi:10.1002/ana.24932
70. Pfyffer D, Huber E, Sutter R, Curt A, Freund P. Tissue bridges predict recovery after traumatic and ischemic thoracic spinal cord injury. *Neurology*. Oct 15 2019;93(16):e1550-e1560. doi:10.1212/wnl.0000000000008318
71. Dienes Z. Using Bayes to get the most out of non-significant results. Methods. *Frontiers in Psychology*. 2014-July-29 2014;5doi:10.3389/fpsyg.2014.00781
72. Kass RE, Raftery AE. Bayes Factors. *Journal of the American Statistical Association*. 1995/06/01 1995;90(430):773-795. doi:10.1080/01621459.1995.10476572
73. Catani M. A little man of some importance. *Brain*. 2017;140(11):3055-3061. doi:10.1093/brain/awx270
74. Flesher SN, Collinger JL, Foldes ST*, et al*. Intracortical microstimulation of human somatosensory cortex. *Sci Transl Med*. Oct 19 2016;8(361):361ra141. doi:10.1126/scitranslmed.aaf8083
75. Bruurmijn M, Pereboom IPL, Vansteensel MJ, Raemaekers MAH, Ramsey NF. Preservation of hand movement representation in the sensorimotor areas of amputees. *Brain*. Dec 1 2017;140(12):3166-3178. doi:10.1093/brain/awx274
76. Andersen RA, Aflalo T. Preserved cortical somatotopic and motor representations in tetraplegic humans. *Current Opinion in Neurobiology*. 2022/06/01/ 2022;74:102547. doi:https://doi.org/10.1016/j.conb.2022.102547
77. Makin TR, Krakauer JW. Against cortical reorganisation. *eLife*. 2023/11/21 2023;12:e84716. doi:10.7554/eLife.84716
78. Armenta Salas M, Bashford L, Kellis S*, et al*. Proprioceptive and cutaneous sensations in humans elicited by intracortical microstimulation. *Elife*. Apr 10 2018;7doi:10.7554/eLife.32904
79. Flesher SN, Downey JE, Weiss JM*, et al*. A brain-computer interface that evokes tactile sensations improves robotic arm control. *Science*. May 21 2021;372(6544):831-836. doi:10.1126/science.abd0380

80. Hiremath SV, Tyler-Kabara EC, Wheeler JJ*, et al*. Human perception of electrical stimulation on the surface of somatosensory cortex. *PLoS One*. 2017;12(5):e0176020. doi:10.1371/journal.pone.0176020
81. Muret D, Makin TR. The homeostatic homunculus: rethinking deprivation-triggered reorganisation. *Current Opinion in Neurobiology*. 2021/04/01/ 2021;67:115-122. doi:https://doi.org/10.1016/j.conb.2020.08.008
82. Muret D, Root V, Kieliba P, Clode D, Makin TR. Beyond body maps: Information content of specific body parts is distributed across the somatosensory homunculus. *Cell Reports*. 2022/03/15/ 2022;38(11):110523. doi:https://doi.org/10.1016/j.celrep.2022.110523
83. Gordon EM, Chauvin RJ, Van AN*, et al*. A somato-cognitive action network alternates with effector regions in motor cortex. *Nature*. 2023/05/01 2023;617(7960):351-359. doi:10.1038/s41586-023-05964-2
84. Jurkiewicz MT, Mikulis DJ, Fehlings MG, Verrier MC. Sensorimotor Cortical Activation in Patients With Cervical Spinal Cord Injury With Persisting Paralysis. *Neurorehabilitation and Neural Repair*. 2010/02/01 2009;24(2):136-140. doi:10.1177/1545968309347680
85. Onifer SM, Zhang YP, Burke DA*, et al*. Adult rat forelimb dysfunction after dorsal cervical spinal cord injury. *Experimental neurology*. 2005;192(1):25-38.
86. Massey JM, Hubscher CH, Wagoner MR*, et al*. Chondroitinase ABC Digestion of the Perineuronal Net Promotes Functional Collateral Sprouting in the Cuneate Nucleus after Cervical Spinal Cord Injury. *The Journal of Neuroscience*. 2006;26(16):4406-4414. doi:10.1523/jneurosci.5467-05.2006
87. Chen LM, Qi HX, Kaas JH. Dynamic reorganization of digit representations in somatosensory cortex of nonhuman primates after spinal cord injury. *J Neurosci*. Oct 17 2012;32(42):14649-63. doi:10.1523/jneurosci.1841-12.2012
88. Dutta A, Kambi N, Raghunathan P, Khushu S, Jain N. Large-scale reorganization of the somatosensory cortex of adult macaque monkeys revealed by fMRI. *Brain Struct Funct*. Jul 2014;219(4):1305-20. doi:10.1007/s00429-013-0569-8
89. Endo T, Spenger C, Tominaga T, Brené S, Olson L. Cortical sensory map rearrangement after spinal cord injury: fMRI responses linked to Nogo signalling. *Brain*. 2007;130(11):2951-2961. doi:10.1093/brain/awm237
90. Root V, Muret D, Arribas M*, et al*. *Investigating facial information content in the hand area of individuals with a congenital and acquired missing hand*. 2021.
91. Stoeckel MC, Seitz RJ, Buetefisch CM. Congenitally altered motor experience alters somatotopic organization of human primary motor cortex. *Proceedings of the National Academy of Sciences*. 2009;106(7):2395-2400. doi:doi:10.1073/pnas.0803733106
92. Kamping S, Lütkenhöner B, Knecht S. Shifting of cortical somatosensory areas in a man with amelia. *Neuroreport*. Oct 25 2004;15(15):2365-8. doi:10.1097/00001756-200410250-00013
93. Hahamy A, Macdonald SN, van den Heiligenberg F*, et al*. Representation of Multiple Body Parts in the Missing-Hand Territory of Congenital One-Handers. *Curr Biol*. May 8 2017;27(9):1350-1355. doi:10.1016/j.cub.2017.03.053
94. Tucciarelli R, Bird L, Straka Z*, et al*. Shaping the developing homunculus: the roles of deprivation and compensatory behaviour in sensory remapping. *bioRxiv*. 2024:2024.11.26.624817. doi:10.1101/2024.11.26.624817

95. Jain N, Florence SL, Qi HX, Kaas JH. Growth of new brainstem connections in adult monkeys with massive sensory loss. *Proc Natl Acad Sci U S A*. May 9 2000;97(10):5546-50. doi:10.1073/pnas.090572597